International Journal of Thermal Sciences 220 (2026) 110293

Contents lists available at ScienceDirect

International Journal of Thermal Sciences

journal homepage: www.elsevier.com/locate/ijts

Thermal diffusivity measurements using dual probe Scanning Thermal Microscopy

Jan Martinek [a,b,*], Václav Hortvík [a], Miroslav Valtr [a], Petr Klapetek [a]

[a] Czech Metrology Institute, Okružní 31, Brno, 638 00, Czech Republic
[b] Faculty of Civil Enginnering, Brno University of Technology, Žižkova 17, Brno, 602 00, Czech Republic

ARTICLE INFO

Keywords:
Thermal diffusivity
Microscopy
Metrology

ABSTRACT

We present a novel dual probe Scanning Thermal Microscopy setup and methodology for addressing measurements of thermal diffusivity using two microscale thermal probes placed at mutual distance between 1 to 60 μm, monitoring propagation of heat pulses from one probe to another one through the studied sample. It is shown that even if the measured heat pulses are very weak in this configuration, they can be measured if the heat transfer via air is reduced by measuring in vacuum, radiative heat transfer is reduced by suitable measurement protocol and many pulses are averaged. Resulting signals show the expected dependencies and thermal diffusivity can be evaluated from them with a help of a numerical modeling. Diffusivity measurements are demonstrated on glasses and polymer samples and potential uncertainty sources are identified.

1. Introduction

Scanning Thermal Microscopy (SThM) is an unique tool for addressing the heat transport phenomena at microscale and nanoscale [1]. Being based on Scanning Probe Microscopy (SPM) technology, it offers very accurate positioning of a nanoscale probe, which, on top of it, is equipped with a temperature sensing element. Most widely used probes are based on use of a microscale resistive heater on the probe apex and can be used to not only sense the temperature but also to heat the sample locally. While measurement regimes for addressing both local sample temperature and local thermal conductivity are used routinely, even if quantitiative measurement is not always easy, thermal diffusivity is not handled very often.

Thermal diffusivity at macroscale is usually measured using either periodic or pulse heating of the sample and monitoring the time dependence of the thermal response at some distance of the heater [2,3]. Both heath sources and sensors can be contact or non-contact, using various principles. A laser flash method, based on heating the sample using laser pulse from one side and monitoring the temperature increase by infrared sensor on the other side is used particularly often, also for metrology purposes [4,5]. Need for monitoring heat flow through some distance and related time phenomena limited use of SThM for thermal diffusivity measurements, however, when an additional source was added, i. e. adding a micro-hotplate below the sample, and using SThM probe was as a sensor, measurements similar to laser flash method were reported [6,7]. Going further to microscale, SThM probes could be used both for excitation and detection, if two of them would be used. Dual probe design and realization for diffusivity measurements, as reported in Ref. [8] are a step in this direction, based on a single probe with two temperature sensing elements. However, no detailed methodology for diffusivity measurements was provided as the paper was focusing on manufacturing aspects. Another option is to use two independent and "standard" SThM probes that would be in a known mutual distance. This approach is explored in our paper.

Use of more than one probe in a SPM is still quite rare and is predominantly used for electrical and optical measurements, e. g. addressing electron transport in low dimensional materials [9] or carrier motion in a quantum well [10]. Less frequently also the other properties are addressed, e. g. critical dimension measurements using dual self-sensing probe setup [11]. In the area between optical and thermal measurements we can find a proposal and theoretical model for thermally excited dual probe near-field radiation measurement in Ref. [12].

This paper presents a relatively simple setup for dual probe SThM measurements, based on use of one stationary probe that can be moved only in z direction (approached and retracted) and one moving probe that can be positioned using a nanopositioning stage like in any other SPM. Distance between the probes can be therefore set using the nanopositioning stage. Both probes are connected to a SThM electronics and both can act as a heat source or heat sink, depending on their temperature. While the device can be operated using different regimes, addressing both thermal conductivity and thermal diffusivity, this paper focuses only on the measurement strategy needed to obtain the

* Corresponding author at: Czech Metrology Institute, Okružní 31, Brno, 638 00, Czech Republic.
E-mail address: jmartinek@cmi.cz (J. Martinek).

https://doi.org/10.1016/j.ijthermalsci.2025.110293
Received 30 May 2025; Received in revised form 19 August 2025; Accepted 3 September 2025
Available online 16 September 2025

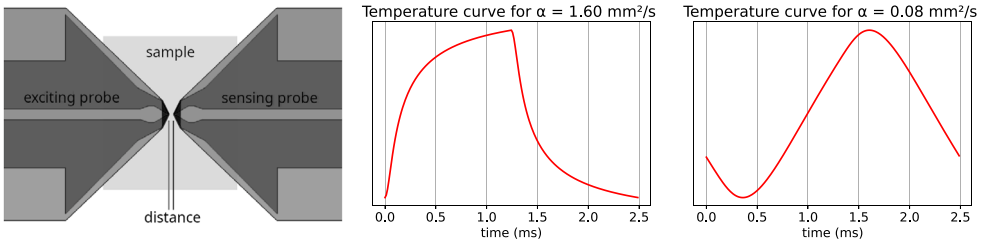

Fig. 1. Measurement principle: (left) Top view of two SThM probes placed at small mutual distance, one sending heat pulses and one detecting them, the temperature profiles expected at measurement of two different samples with hypothetical thermal diffusivities $\alpha = 1.60\,\mathrm{mm^2/s}$ (middle) and $\alpha = 0.08\,\mathrm{mm^2/s}$ (right). For all other measurement conditions being the same, the temperature curve shape depends on thermal diffusivity.

diffusivity related signals, which could, at first sight, look as a simplest regime in terms of data acquisition and interpretation. Therefore, here one of the probes is always used as a source of heat pulses and second one as a sensor.

2. Measurement principle

The basic idea of diffusivity measurements is the same as for the laser flash method. A pulse is generated by one of the probes ("exciting" probe) and its evolution in time at certain distance is monitored by the second probe ("sensing" probe). The time needed for the heat wave to pass from one probe depends on the distance between the probes and on the sample diffusivity and similarly to that, the shape of the detected pulse changes, which can be detected and diffusivity can be evaluated from it with help of numerical modeling. Calibration of the probes is not required, as the temperature unit (Kelvin) does not appear in the measurements, computations, or results. Thermal diffusivity is expressed in units of m^2/s, which do not involve temperature. This is analogous to the well-established laser flash method, where calibrated temperature sensors are likewise unnecessary. To illustrate what happens with a pulse when passed through the sample we plot a dependence of a detected pulse shape on the diffusivity, at constant probe-probe distance, in Fig. 1, as computed using Finite Element Method. The computational details will be described later in the paper, but to illustrate the basic idea, let us consider a square voltage signal driving a SThM probe at a frequency of 400 Hz, with a second probe located 20 μm away sensing the resulting temperature profile. The shape of the sampled temperature curve depends on the thermal diffusivity of the material, distance between the probes and pulse frequency. An example for two diffusivities (with other parameters fixed) is shown in Fig. 1.

3. Experimental arrangement

For our measurements, we have developed a custom built dual probe vacuum setup as going to vacuum turned to be necessary after first experiments in air, where we found that the air probe-probe heat transfer easily dominates all the signals, similarly as observed for dual SThM probe in Ref. [8]. Reducing the air pressure to about 6 Pa allowed us to reduce this effect massively.

The whole measurement setup is shown in Fig. 2. The primary goal of the design was to keep as many of the components out of the vacuum part, namely when it comes to the probe-sample feedback. The probe-sample interaction sensing unit (A) and optical microscopes (B) are therefore mounted outside of the vacuum chamber, above a glass window (D), while the two probes and sample are located about 5 mm below this window, inside the vacuum chamber. Only one probe (H), in this work being used as the sensing one, uses a laser based feedback, therefore it is mounted not to be moving with respect to the laser deflection detection system (except of use of z axis piezo actuator). The optical deflection pickup related to probe H is connected to Gwyscope SPM controller [13] which is used for the feedback. The second probe (F) and sample are mounted on a coarse XYZ stage (Smaract) combined with piezo actuated stage (Physik Instrumente, G) which is used for movement to the area of interest and for approach to the feedback. This probe is used as exciting probe and is mounted on an additional XYZ actuator (Thorlabs) in order to align it with respect to the sample. During the scan, both sample and one of the probes are moving during scan while the sensing does not move laterally to keep the feedback laser aligned to it.

One of the probes, referred to as the exciting probe, is connected to the output of the measurement card, which generates square pulses. As a result, the probe periodically heats up and cools down. Most samples were measured at a pulse frequency of 400 Hz. The amplitude was set relatively high to ensure a strong signal, while still avoiding damage to the driven probe, which may reach temperatures well above 100 °C.

The signal measured by sensing probe is generally very weak — much weaker than the noise. Within a single acquisition period, the useful information is completely obscured. Fortunately, the signal is periodic, and both its period and phase are known, as it is synchronized with the square-wave thermal pulses generated at the excitation probe. This makes it straightforward to continuously acquire data by sampling successive periods and averaging the results, thereby enhancing the signal-to-noise ratio. Our typical measurement consists of 400,000 sampled and averaged periods, and with such a high number, the signal curve gradually begins to emerge. The sample temperature rises over time, and as a result, the mean level of the signal exhibits a slow drift. However, the averaging process still yields valid results, since each individual period is sufficiently short that the temperature rise within a single period remains minimal. Consequently, the transient drift affects the baseline but does not compromise the reliability of the averaged signal. The result of the measurement is a transient temperature curve, which is then compared with the corresponding result obtained from FEM simulations. Alternatively, only the amplitude and phase could be extracted using lock-in detection. In order to keep the background noise as low as possible, custom electronics has been made to process the signal from the sensing probe. The first stage is a Wheatstone bridge. In one of the branches of the bridge there is the SThM probe whose resistance responds to temperature. The bridge must be excited in order to operate which was done using a suitable voltage reference. Slight variations of temperature result in differential signal in the bridge which is amplified by low noise instrumentation amplifier AD8429. The electronics is battery powered in order to avoid interference from mains and to provide galvanically isolated supply to interrupt eventual ground loops. The voltage from the batteries is further stabilized using a pair of ultra-low noise voltage regulators LT3045 and LT3094 providing symmetric voltage. All the electronics is thoroughly shielded including the wires, connectors and the whole chamber. The exciting probe is connected to the output of a National Instruments PCI-6010 measurement card, while the sensing probe, through its amplifier, delivers the signal to the input of the same card.

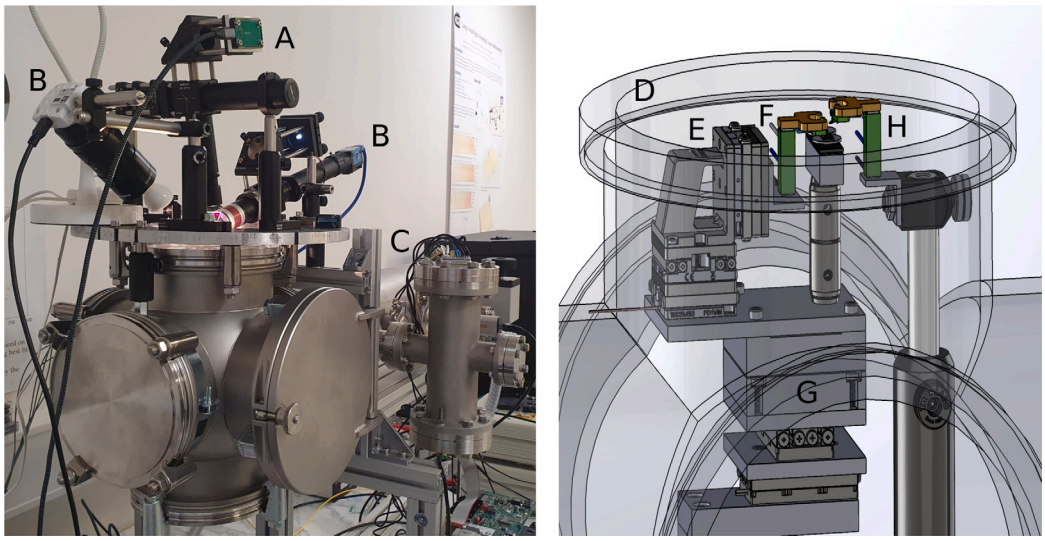

Fig. 2. Dual probe vacuum system overview: A: AFM laser feedback module, B: camera, C: vacuum chambers and feedthroughs, D: glass window, E: probe 1 XYZ stick–slip actuator, F: probe 1 and its piezo actuator, G: probe 1 + sample XYZ piezo and stick-skip actuator, H: probe 2 and its piezo actuator.

4. Measurement protocol

To address the weak signals related to temperature pulse passing from one probe, through sample, to the second probe, we had to remove as many of the potential parasitic heat flow paths as possible. Pressure in the chamber was reduced to 6 Pa to minimize the impact of probe-probe air conduction. To reduce impact of air residuals and of probe-probe radiation, measurements were always performed with both probes in contact (“on” measurement) and with one probe out of contact, in distance of 5 μm from the surface (“off” measurement) and these two datasets were subtracted.

As discussed above, we assume that a sudden change of thermal power of one SThM probe will induce a time-space evolution of temperature field in the vicinity of the probe and is detectable by the second probe nearby. As the signal is very weak, this needs a lot of averaging across multiple pulses. To obtain an accurate response, the driving signal and the detected signal must be well synchronized. For this purpose, a National Instruments measurement card PCI-6010 with analog input and output was used, and custom-made software was developed to control the signals. The analog output was directly connected to the driven SThM probe and programmed to generate a square wave with an amplitude sufficient to heat the probe and a suitable frequency. The analog input measured the thermal response of the moving probe. The sampling frequency was set to 1.25 MHz, with both the input and output channels derived from the same internal clock. The synchronization of both channels was verified by directly interconnecting the input and output. After adjusting the time constants, excellent timing precision was achieved, with the rise and fall edges detected at the same sample, i. e., better than 1 microsecond.

The measurement protocol was as follows:

1. Sample was placed to the vacuum chamber, vacuum was established and a clean and flat area on the sample was selected using an optical microscope.
2. Synchronization between the input and output signals was adjusted and verified by temporarily routing the output signal directly into the input.
3. Exciting probe was landed to the sample using stick–slip actuator and piezoelectric transducer, monitoring the SThM signal using a standard Wheatstone bridge based electronics to see the jump to the contact and then is re-connected to data acquisition card input via amplifier.
4. Sensing probe was landed to the sample at a distance of about 60 μm from the exciting probe, based on the optical microscope image and stayed in the SPM contact mode feedback.
5. For each measurement point, few profiles perpendicular to the probe-probe axis were performed to cross-check if there is no contact between the probes (which could be seen on error signal, topography and in some cases even on the optical image) and probe was left at some particular position.
6. Measurement was performed, obtaining the “on” dataset.
7. Sensing probe was retracted and measurement was repeated, obtaining the “off” dataset.
8. Sensing probe was moved closer to the exciting probe using the nanopositioning stage and the whole process (4–6) was repeated until a contact between the probes was identified. When this happened, the contact position was noted as the zero position.
9. At the end of the measurement, the sensing probe was retracted. Exciting probe was connected back to the Wheatstone bridge electronics and retracted as well, cross-checking the presence of a jump in the thermal signal to prove that the contact to the surface was kept the same during the measurement.

Using the above procedure we obtained a set of “on” and “off” datasets at different known distances between the probes.

5. Data evaluation

In the previous section it was shown that the temperature curve depends on thermal diffusivity if pulse frequency and distance between the probes is the same. To further investigate the temperature field evolution the heat conduction equation was solved.

$$\frac{\partial T}{\partial t} = \alpha \, \Delta T \tag{1}$$

In the heat conduction equation, T denotes temperature; however, since the equation is valid for any temperature scale, calibration of the probes is not required. The solution and the fundamental properties of the equation reveal that the temperature curve changes in the same manner not only by different material but also by varying the distance between the probes or by varying the pulse frequency. Since this property is important for data processing, it might be useful to look at the profiles in more details. The graphs in Fig. 3 represent the temperature curve for various distances between the probes for the same pulse frequency and the same sample.

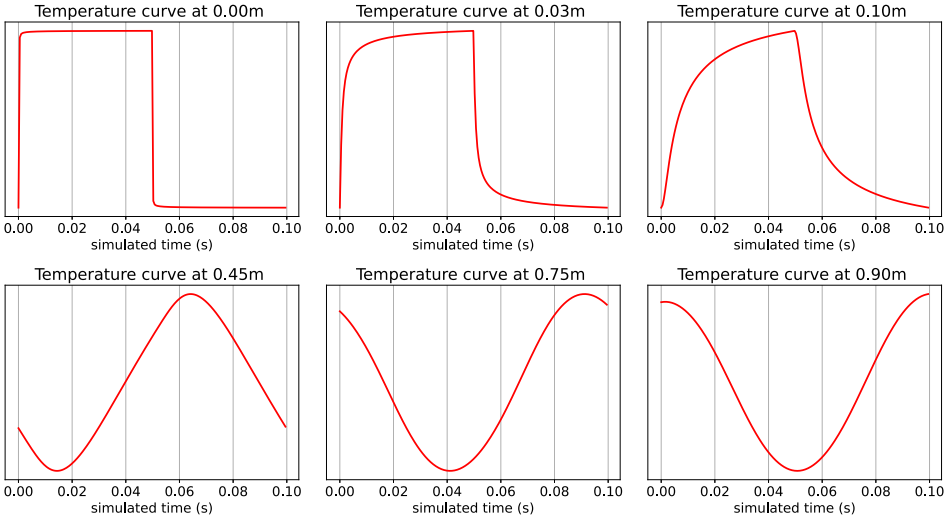

Fig. 3. Simulated temperature curve at various distances between probes. The calculated solution of the heat conduction equation was performed for a hypothetical material with unity $\alpha = 1\,\mathrm{m}^2/\mathrm{s}$ and pulse frequency $f = 10\,\mathrm{Hz}$. All three parameters — distance, time and thermal diffusivity — are meant to be scaled to realistic values.

As shown in the graphs, the temperature response curve depends on the distance between the probes. At very short distances, the curve is nearly square-shaped, as the measuring probe closely follows the temperature of the driven probe. With a slight increase in distance, the curve begins to resemble rising and falling exponentials. This trend becomes more pronounced with further separation. At even greater distances, the temperature curve becomes triangular, and with further increases in the gap, it gradually converges into a sinusoidal shape. A noticeable increase in phase lag is also observed. These effects have been used to match the measured curve with one of the simulated curves. Although the amplitude also decreases with increasing distance between the probes, this phenomenon was not taken into account, as it strongly depends on local interactions between the probe and the surface.

The heat conduction equation was solved numerically using the Finite Element Method. Since the heat from the driven probe spreads axisymmetrically, the simulation domain was modeled as a simple cylinder with the heat source located at the center of the upper face. To reduce computation time, the problem was further simplified to a 2D cross-sectional model, taking advantage of axial symmetry.

The computational domain was defined as a simple rectangle representing the cross-section of a cylinder. A non-uniform mesh was used, with the highest density located at the corner of the rectangle where the steepest temperature gradient is expected — corresponding to the position of the heating probe.

To keep the model manageable, the probes were not explicitly included. In practice, however, their presence introduces both thermal contact resistance and thermal inertia due to their mass. These effects influence the amplitude of temperature oscillations (and thus the signal strength), as well as the time delay and the shape of the transient temperature curve.

While an ideal model would account for all such effects, including pulsed heating, incorporating every physical detail — along with independently measured parameters of sufficient accuracy — would render the computation and overall methodology prohibitively complex. As a result, we introduced simplifications that preserve agreement with the experimental data.

A particularly valuable insight was gained by placing both probes in direct contact, i.e., with zero gap between them. In the absence of thermal inertia and other parasitic effects, the system's response to periodic heating would produce a rectangular waveform. The observed response curve, however, was distorted, clearly indicating the presence of such effects.

To capture this behavior in the model, we introduced a localized modification. Several elements near the heating probe were assigned a different material to simulate the region affected by thermal inertia. This subdomain, on the order of tens of nanometers in size, incorporated internal heat sources rather than step temperature changes, thereby modeling a finite heating rate. Additionally, the zero-point of the measurement was slightly shifted away from the heating probe to represent further delay caused by thermal inertia.

After fine-tuning the sizes and material constants, the model achieved good agreement with the experimentally observed thermal response. While the detailed geometry and material properties of the probes were not explicitly modeled, the overall physical behavior — including signal delay and deformation — was successfully reproduced.

Each probe is characterized by its own response, and a finite thermal resistance exists at the probe–sample interface. These factors play a significant role in the measurements, as they strongly influence the shape of the response curves that are essential for data processing. A key assumption in our approach is that the contact resistance remains constant between the zero-gap configuration and the actual measurement. While the influence of both the probe response and the contact resistance is undeniable, their explicit numerical values are not required for the present analysis. Furthermore, incorporation of the thermal resistance is not feasible, as its unit (K/W) involves the temperature scale, and the probes are not calibrated.

The FEM mesh consisted of approximately 120,000 elements, with the highest density concentrated around the probe locations. The surrounding region was more sparsely meshed to approximate an effectively infinite sample. The temperature curve was evaluated at 1000 points along the edge where the sensing probe is expected to be located. Since the model dimensions are rescaled during later evaluations, it is not possible to specify the exact spacing between these evaluation points. However, in all cases, the resolution is better than 100 nm.

The overall simulation consisted of 2000 time steps, representing 10 square pulse periods. Each period therefore comprised 200 time steps. For further analysis, only the shape of the final period was used, as the oscillations were found to stabilize after approximately 10 periods.

The boundary condition at the edge where the probes are located was set to adiabatic. The remaining edges represent the limits of the computational domain, while the sample itself is considered semi-infinite. Various boundary conditions were tested, and since their influence on the results was minimal, this confirms that the domain size was sufficiently large to accurately represent a sample extending

beyond the model boundaries. However, at least some of the boundaries should be set to isothermal to represent a heat sink and prevent the overall temperature of the domain from increasing indefinitely.

Although we used a supercomputer, the problem involves time-dependent evolution, where each step depends on the previous one. This type of computation is inherently difficult to parallelize, so the availability of a large number of CPU cores provides only limited benefit. For this reason, it was important to keep the model as simple and efficient as possible.

The simulation produced temperature response curves calculated for a series of points at increasing distances between the probes. For FEM modeling, we chose an open-source solution to allow for full customization of the toolchain to meet our specific needs. This approach is not only free but also highly flexible. We used a combination of the Python programming language and SfePy — a Python module that supports finite element modeling. SfePy is not a standalone software package; rather, it is primarily a computational library designed for solving partial differential equations.

However, the heat conduction equation cannot be solved directly because the thermal diffusivity, α, is unknown. In theory, the computation could be performed iteratively by varying this unknown parameter until the resulting curve matches the measured one. Instead, a much more efficient approach was adopted.

The heat conduction equation yields the same solution for any given Fourier number, $F_o = \alpha t / L^2$, where t is time and L is the characteristic length scale of the problem. All three parameters — α, t, and L — can be arbitrarily scaled by a common factor without altering the solution, as long as the Fourier number remains constant. By exploiting this property, the simulation needs to be performed only once to obtain $T(x,t)$, i. e., the spatial and temporal temperature distribution. The frequency of the square pulses, the thermal diffusivity, and the domain size were initially chosen arbitrarily to ensure numerical stability. These parameters can then be rescaled to match the experimental data.

The same temperature profile is obtained if the Fourier number is the same for the measured data and simulation.

$$\frac{\alpha_m t_m}{L_m^2} = \frac{\alpha_s t_s}{L_s^2} \tag{2}$$

From this relationship, the unknown thermal diffusivity can be expressed as:

$$\alpha_m = \frac{t_s}{t_m}\left(\frac{L_m}{L_s}\right)^2 \alpha_s \tag{3}$$

The only unknown variable, simulated distance L_s, was determined by comparing the simulated temperature profiles with the measured data. The best match was identified using the least squares method.

6. Materials and limitations

At first, suitable samples to be tested were chosen. This, however, is complicated as some materials are more difficult to be measured and our setup has its limitations.

There are two main challenges. The first is difficult to avoid and relates to the weak signal, whose signal-to-noise ratio cannot be further improved by increasing the measurement time due to the positional drift of the SThM probe. The second challenge involves the thermal inertia of the probes and the thermal contact resistance. This undesired effect can be accounted for by measuring the actual response of the entire setup and adjusting the FEM model to reproduce this behavior.

We have further investigated the measurement method to find out its limitations. The signal can be made stronger if the contact resistance is decreased. This has been confirmed using PCL, polycaprolactone. The probe slightly melted into the material making the thermal contact better thus improving its strength. This approach is mostly unusable, but the use of PCL demonstrates the principle. Another way to increase the signal strength is to decrease the distance between the probes. However, this approach has two drawbacks. First, the probe positions are known with a certain absolute error, and as the distance between them decreases, the relative error increases. Second, the thermal inertia of the probes has a more pronounced effect at shorter distances. Although this issue can be partially mitigated during data processing, it is preferable to minimize its impact through the experimental setup.

In addition, the signal level also depends on the material being tested, which presents a limitation of the method or, more specifically, our experimental setup. Some materials are inherently more suitable for this type of measurement. In general, increasing the temperature swing amplitude at the sensing probe improves signal quality. However, the situation is complex. Assuming the thermal resistances remain constant and the voltage pulse at the driving probe is unchanged, the resulting signal level depends on both the thermal conductivity and the volumetric heat capacity of the material. Since volumetric heat capacity tends to vary less across materials, thermal conductivity becomes the dominant factor. For simplicity, we consider materials with high thermal conductivity to be more challenging for accurate measurement. Among the many materials we tested, only a few were suitable. Notably, certain well-defined reference materials — such as single-crystal silicon — could not be used due to their high thermal conductivity.

7. Results

The following samples were measured: molded lens from Thorlabs made of polymethyl methacrylate (PMMA), BK7 glass from Thorlabs and Bruker reference sample for nano-thermal analysis (VITA-CS-NANOTA sample), consisting of thin sheets of PCL, HDPE and PET - only PCL is presented here.

Each material has been tested for several distances between the probes thus obtaining curves which lead to calculation of thermal diffusivity. Each individual results, however, has its uncertainty found using the law of uncertainty propagation derived from Eq. (3). There are two main sources of error — both related to the distance between the probes. The first source of uncertainty arises from the positional drift during the experiment. The probe distance is known with an accuracy of approximately one micrometer, and due to drift, higher precision cannot be guaranteed. The second source of uncertainty stems from fitting noisy experimental data and aligning it with the simulated curve. Despite the high noise level, the fitting procedure reliably identifies the correct FEM node at which the curve is evaluated. We estimate the uncertainty in this step to correspond to one FEM node. The physical units are not critical, as only the relative error is used in the calculations.

Results for polymethyl methacrylate (PMMA) are shown in Fig. 4. As we can see from the individual results in the figure caption, every single measurement and data fitting provides a diffusivity value. Performing set of measurements at different probe-probe distances can be used to validate the approach and to search for potential parasitic effects. After calculating the mean and standard error from all measured values — including those not shown in the graphs — the following results were obtained for PMMA: $\alpha = (0.1103 \pm 0.0050)\,\mathrm{mm^2/s}$.

The reference values of the relevant material constants, required for evaluating the accuracy of the measured data, are not readily available. The published results often vary depending on measurement method and slight differences in seemingly the same material, like purity, crystallinity, method of preparation, etc. In the case of PMMA, we can rely on the intercomparison data of thermal diffusivity measurements published in [14]. All values obtained using our method fall within the confidence intervals reported by at least some of the participating laboratories. Moreover, the referenced paper also indicates that thermal diffusivity decreases with increasing temperature. At approximately room temperature, the value can be estimated from their graph as $\alpha = (0.113 \pm 0.015)\,\mathrm{mm^2/s}$.

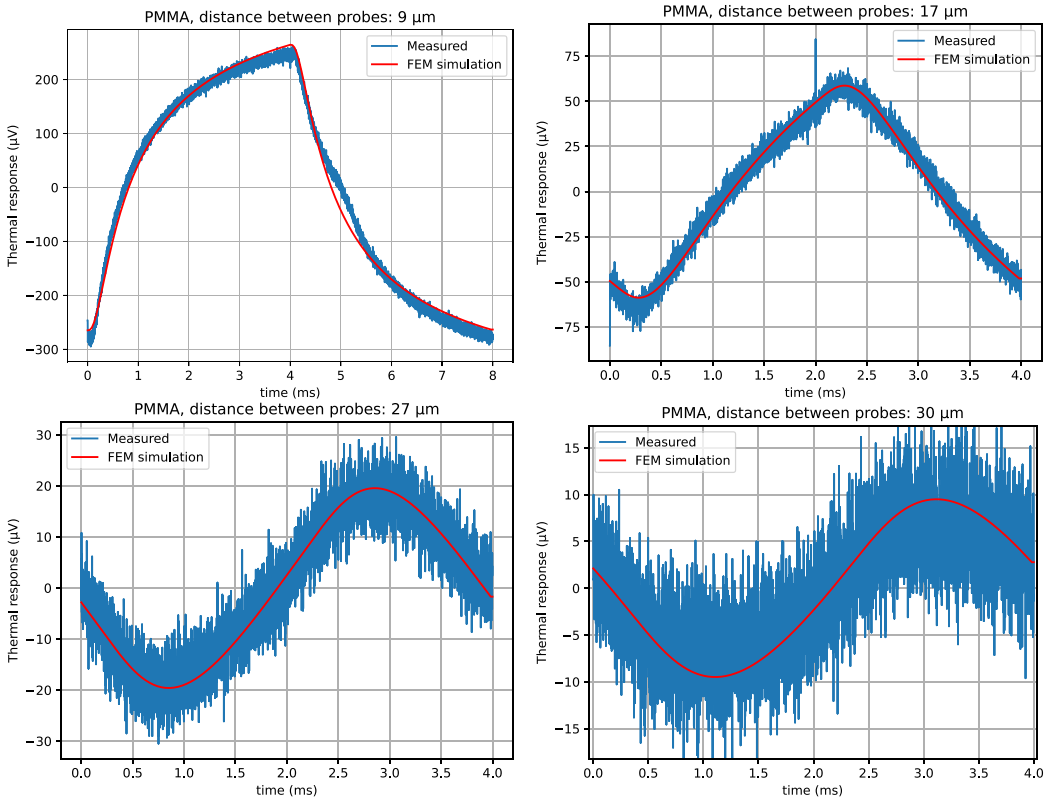

Fig. 4. Examples of measured and simulated temperature curves for PMMA at distances between the probes 9 µm, 17 µm, 27 µm and 30 µm. The calculated thermal diffusivities are $(0.125 \pm 0.030)\,\mathrm{mm}^2/\mathrm{s}$, $(0.097 \pm 0.014)\,\mathrm{mm}^2/\mathrm{s}$, $(0.104 \pm 0.011)\,\mathrm{mm}^2/\mathrm{s}$, and $(0.116 \pm 0.010)\,\mathrm{mm}^2/\mathrm{s}$, respectively.

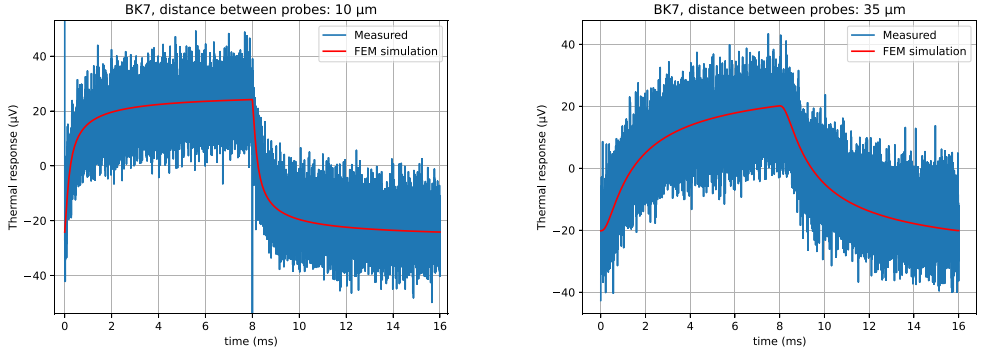

Fig. 5. An example of two measured and simulated temperature curves for BK7 glass at distances between the probes 10 µm and 35 µm. The calculated thermal diffusivities are $(0.54 \pm 0.11)\,\mathrm{mm}^2/\mathrm{s}$ and $(0.49 \pm 0.056)\,\mathrm{mm}^2/\mathrm{s}$, respectively.

The next material chosen for the measurement was borosilicate glass BK7, see the graphs in Fig. 5.

The measured thermal diffusivity yields a significantly higher value than that of PMMA, which is expected. An independently measured value, published in [15], is $0.548\,\mathrm{mm}^2/\mathrm{s}$. According to another source [16], which employed two different methods, the reported values are $(0.538 \pm 0.027)\,\mathrm{mm}^2/\mathrm{s}$ and $(0.540 \pm 0.027)\,\mathrm{mm}^2/\mathrm{s}$. After processing all of our measured data, we obtained a thermal diffusivity for BK7 glass of $\alpha = (0.502 \pm 0.042)\,\mathrm{mm}^2/\mathrm{s}$, which is in agreement with the latter published values.

The third material tested was polycaprolactone (PCL). In this case, the results are likely influenced by its low melting point and potential phase transitions, which can significantly affect the measurements. As shown in Fig. 6, the signal is exceptionally strong — much stronger than in all other measurements. While this is advantageous for data processing, the increased signal strength may result from the probes partially melting into the material, thereby enhancing thermal transport. As a consequence, the calculated thermal diffusivities are difficult to compare directly with reference data. Nevertheless, the obtained values are at least within the typical range for most polymers. From all the measurements we get this result for PCL: $\alpha = (0.1020 \pm 0.0049)\,\mathrm{mm}^2/\mathrm{s}$.

8. Discussion

Due to lack of suitable reference materials, we could compare our results only to table values that have relatively broad ranges. Even if the measured results fit to these values, we can see that there is some variance in the experimental data, e. g. when evaluating them from different probe-probe distances, that needs to be discussed when it comes to the measurement uncertainty. Here we try to identify the

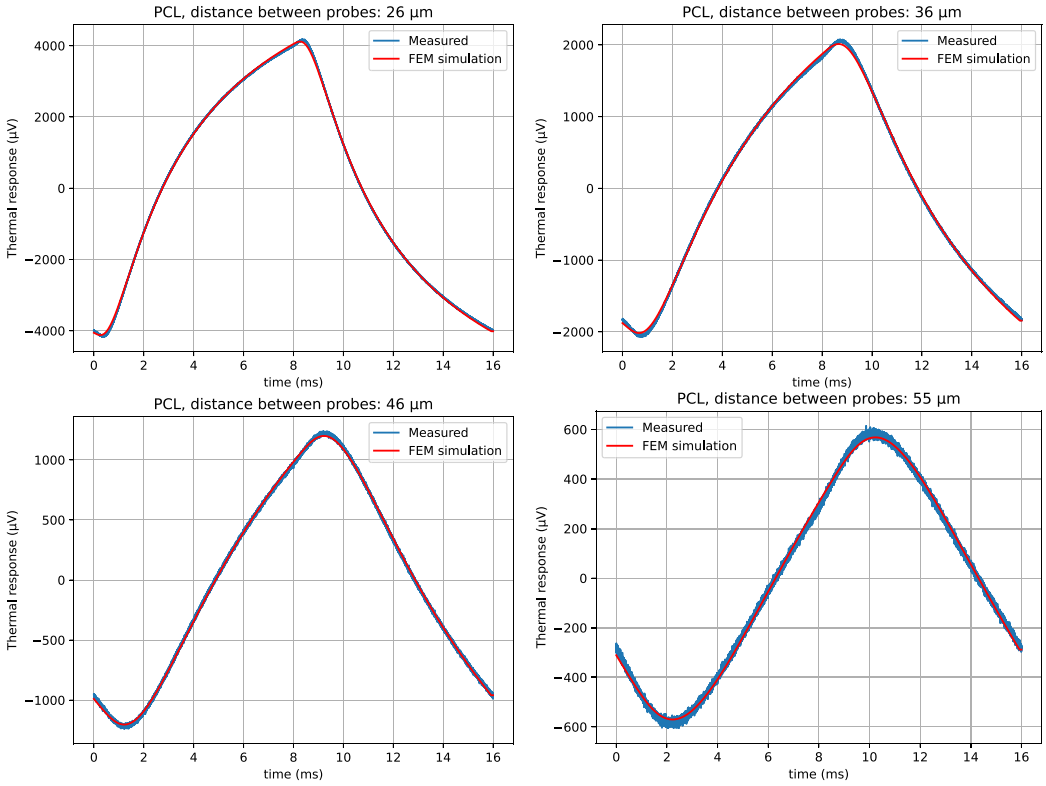

Fig. 6. Measured and simulated temperature curves for PCL at distances between the probes 26 µm, 36 µm, 46 µm and 55 µm. The calculated thermal diffusivities are $(0.096 \pm 0.015)\,\mathrm{mm}^2/\mathrm{s}$, $(0.104 \pm 0.012)\,\mathrm{mm}^2/\mathrm{s}$, $(0.1105 \pm 0.0096)\,\mathrm{mm}^2/\mathrm{s}$, and $(0.0981 \pm 0.0071)\,\mathrm{mm}^2/\mathrm{s}$, respectively.

potential uncertainty components. Some of them were found to be negligible, but some should be still addressed in our future work.

- Another problem to address is how to determine the probe-probe distance. Here we can rely on the nanopositioning systems used in SPM, which are typically accurate up to few nanometers. We only need to know the mutual position of the probes once and then to use the nanopositioning stage. We experienced that the KNT probes are sufficiently robust to scan one probe by another one, when they are both in contact with the surface, so the zero position can be obtained by scanning the apex of fixed probe by the moving probe. The uncertainty of the probe-probe distance in the rest of the experiment depends on positioning accuracy and on the mechanical and thermal stability of the setup. Determining the zero position by scanning probe on probe can be done with uncertainty far below a single micrometer. However in most of our diffusivity measurements we did not fully scan the probe on probe and we have only identified a position where probes apparently started touching, based on the error signal of the moving probe and used it as a zero position. Therefore, the zero position uncertainty is higher than what would be achievable otherwise. As the measurements were relatively long (fifteen minutes for a single accumulated measurement), when this zero position uncertainty is combined long term mechanical and thermal drifts, its impact on probe-probe position is estimated to be in a single micrometer level. Comparing to these effects, the impact of positioning accuracy of a commercial closed loop nano-positioning system was negligible.
- Probe-sample force for the exciting (stationary) probe was not controlled — probe was approached using piezo actuator and monitoring the thermal signal rise when jumping into contact. After that it was kept at constant z position. After the measurement, the presence of probe-sample contact was again verified by monitoring the signal drop when retracting the probe. The contact force during the measurement could therefore vary. However, the measurements of thermal response vs. probe z position showed very flat region of probe-sample heat flux for different contact forces due to fact that the probe stiffness is very small. Moreover, the measurement results were not evaluated from the signal strength that might be still slightly affected by probe-sample contact variation, but from the signal shape, which is related to the time phenomena.
- Some of the polymer samples featured relatively low melting temperatures. When the probe was heated, sample could be locally softened which affected the contact. If the probe temperature would be high enough, sample could be locally melted and the heat capacity needed for this process would contribute to the results. However for all measurements except polycaprolactone (melting point 60 °C), we have not observed that the probes would mechanically behave other way than on solid samples — they could be scanned and retracted with any apparent increase of adhesion, so we believe that impact of this effect was not large. Nevertheless we cannot quantify it at the moment.
- In order to increase the sensitivity, the sensing probe is also heated by a DC current passing through it. As the sensing probe is placed at different distances from the exciting probe during the measurement, diffusivity is measured always at elevated sample temperature and this temperature slightly depends on the probe-probe distance. This adds some uncertainty to the results as the diffusivity is not constant with the temperature.

Most of the above effects could be addressed by refining the measurement protocol (to control better probe positions), improving the numerical simulations (to include probe time response and to estimate the impact of DC heating) or by improving sensitivity of the measurement (to reduce the temperatures in the setup). This is planned as a future work together with determination of the full uncertainty budget for the method.

9. Conclusion

We have developed a measurement setup and a methodology for measurement of thermal diffusivity at microscale using dual probe Scanning Thermal Microscopy. Our approach is based on sending heat pulses from one probe to the another one through the measured sample, accumulating signal from a very large number of pulses, working in vacuum to reduce impact of heat transfer via air and using on-off methodology to subtract the impact of radiative heat transfer. Data are interpreted with help of a Finite Element Method, simulating the sensing probe signal shape and fitting it to the experimental data. We have validated the concept by performing measurement at different distances between the exciting and sensing probe and by measurements of thermal diffusivities of different bulk materials and comparing the results to table values.

CRediT authorship contribution statement

Jan Martinek: Writing – review & editing, Writing – original draft, Visualization, Validation, Software, Methodology, Formal analysis, Data curation, Conceptualization. **Václav Hortvík:** Supervision, Resources, Methodology, Data curation, Conceptualization. **Miroslav Valtr:** Writing – review & editing, Writing – original draft, Visualization, Validation, Supervision, Software, Methodology, Investigation, Formal analysis, Data curation, Conceptualization. **Petr Klapetek:** Writing – review & editing, Writing – original draft, Visualization, Validation, Supervision, Software, Resources, Project administration, Methodology, Investigation, Funding acquisition, Formal analysis, Data curation, Conceptualization.

Declaration of competing interest

The authors declare that they have no known competing financial interests or personal relationships that could have appeared to influence the work reported in this paper.

Acknowledgments

This work was supported by the Czech Science Foundation project GA23-06263S. This work was also partly funded by Institutional Subsidy for Long-Term Conceptual Development of a Research Organization granted to the Czech Metrology Institute by the Ministry of Industry and Trade.

Data availability

Data will be made available on request.

References

[1] S. Gomès, A. Assy, P.-O. Chapuis, Scanning thermal microscopy: A review, Phys. Status Solidi (A) 212 (3) (2015) 477–494, http://dx.doi.org/10.1002/pssa.201400360, arXiv:https://onlinelibrary.wiley.com/doi/pdf/10.1002/pssa.201400360 URL https://onlinelibrary.wiley.com/doi/abs/10.1002/pssa.201400360.

[2] R. Sundar, C. Sudha, Thermal transport and thermal diffusivity by laser flash technique: A review, Int. J. Thermophys. 46 (1) (2024) 13, http://dx.doi.org/10.1007/s10765-024-03479-0.

[3] R. Taylor, J. Gembarovic, K. Maglic, Thermal diffusivity by the laser flash technique, 2002, http://dx.doi.org/10.1002/0471266965.com102.

[4] J. Blumm, The laser flash technique: A widespread technology for measurement of the thermal diffusivity of solids and liquids, Int. J. Thermophys. 46 (2025) http://dx.doi.org/10.1007/s10765-025-03510.

[5] B. Hay, G. Davee, J. Hameury, O. Enouf, L. Rongione, Détermination de la diffusivité thermique et de la conductivité thermique de revêtements à haute température par la méthode flash, 2011, URL https://api.semanticscholar.org/CorpusID:102222283.

[6] A. Dawson, M. Rides, A.S. Maxwell, A. Cuenat, A.R. Samano, Scanning thermal microscopy techniques for polymeric thin films using temperature contrast mode to measure thermal diffusivity and a novel approach in conductivity contrast mode to the mapping of thermally conductive particles, Polym. Test. 41 (2015) 198–208, http://dx.doi.org/10.1016/j.polymertesting.2014.11.008, URL https://www.sciencedirect.com/science/article/pii/S0142941814002578.

[7] D. Varandani, K. Agarwal, J. Brugger, B.R. Mehta, Scanning thermal probe microscope method for the determination of thermal diffusivity of nanocomposite thin films, Rev. Sci. Instrum. 87 (8) (2016) 084903, http://dx.doi.org/10.1063/1.4960332, arXiv:https://pubs.aip.org/aip/rsi/article-pdf/doi/10.1063/1.4960332/16096304/084903_1_online.pdf.

[8] Y. Zhang, P. Dobson, J. Weaver, Batch fabricated dual cantilever resistive probe for scanning thermal microscopy, Microelectron. Eng. - Microelectron. Eng. 88 (2011) 2435–2438, http://dx.doi.org/10.1016/j.mee.2011.02.040.

[9] A.-P. Li, K. Clark, X. Zhang, A. Baddorf, Electron transport at the nanometer-scale spatially revealed by four-probe scanning tunneling microscopy, Adv. Funct. Mater. 23 (2013) 2509, http://dx.doi.org/10.1002/adfm.201203423.

[10] A. Kaneta, R. Fujimoto, T. Hashimoto, K. Nishimura, M. Funato, Y. Kawakami, Instrumentation for dual-probe scanning near-field optical microscopy, Rev. Sci. Instrum. 83 (8) (2012) 083709, http://dx.doi.org/10.1063/1.4737883, arXiv:https://pubs.aip.org/aip/rsi/article-pdf/doi/10.1063/1.4737883/14832820/083709_1_online.pdf.

[11] Z. Zheng, S. Gao, W. Li, X. Liu, Y. Shi, C. Chen, Dual-probe atomic force microscopy based on tuning fork probes for critical dimension metrology, Ultramicroscopy 219 (2020) 113120, http://dx.doi.org/10.1016/j.ultramic.2020.113120.

[12] J. Chen, B. Wang, C. Zhao, Scattering-type multi-probe scanning thermal microscope based on near-field thermal radiation, Int. J. Heat Mass Transfer 181 (2021) 121869, http://dx.doi.org/10.1016/j.ijheatmasstransfer.2021.121869, URL https://www.sciencedirect.com/science/article/pii/S0017931021009741.

[13] M. Valtr, P. Klapetek, J. Martinek, O. Novotný, Z. Jelínek, V. Hortvík, D. Nečas, Scanning probe microscopy controller with advanced sampling support, HardwareX 15 (2023) e00451, http://dx.doi.org/10.1016/j.ohx.2023.e00451, URL https://www.sciencedirect.com/science/article/pii/S2468067223000585.

[14] M. Rohde, F. Hemberger, T. Bauer, J. Blumm, T. Fend, T. Häusler, U. Hammerschmidt, W. Hohenauer, K. Jaenicke-Rössler, E. Kaschnitz, E. Pfaff, G. Pintsuk, Intercomparison of thermal diffusivity measurements on cucrzr and pmma, High Temp. - High Press. 42 (2014).

[15] L'udovít Kubičár, V. Vretenár, U. Hammerschmidt, Thermophysical parameters of optical glass bk7 measured by the pulse transient method, Int. J. Thermophys. 26 (2) (2005) 507–518, http://dx.doi.org/10.1007/s10765-005-4512-y.

[16] F. Hemberger, A. Göbel, H.-P. Ebert, Determination of the thermal diffusivity of electrically non-conductive solids in the temperature range from 80 k to 300 k by laser-flash measurement, Int. J. Thermophys. 31 (6) (2010) 2187–2200, http://dx.doi.org/10.1007/s10765-010-0876-8.